

10th Deep Sea Offshore Wind R&D Conference, DeepWind'2013

Dynamic analysis of floating wind turbines during pitch actuator fault, grid loss, and shutdown

Erin E. Bachynski^{a,b,*}, Mahmoud Etemaddar^a, Marit I. Kvittem^{a,b}, Chenyu Luan^{a,b},
Torgeir Moan^{a,b}

^aCentre for Ships and Ocean Structures, NTNU, NO-7491 Trondheim, Norway

^bNOWITECH, NTNU, NO-7491 Trondheim, Norway

Abstract

Coupled non-linear aero-hydro-servo-elastic simulations of three types of floating wind turbines (spar, semi-submersible, and tension leg platform) are carried out for several fault cases over a range of environmental conditions based on correlated wind and wave data from the North Sea. Three particular fault scenarios are considered: 1) blade seize, where the pitch actuator of one blade is blocked, 2) blade seize, recognized by the controller and followed by shutdown (grid disconnection and aerodynamic braking), and 3) grid loss followed by shutdown. The platform motions and structural loads caused by fault events are compared to loads encountered during normal operation and during selected extreme weather conditions. Although the global motions and mooring line loads tend to be largest during storm conditions, selected platforms experience large pitch or yaw motions due to blade seize and shutdown. Imbalance loads due to blade seize can lead to particularly large loads on the blades and tower, and the shutdown process can impose relatively large edgewise blade loads.

© 2013 The Authors. Published by Elsevier Ltd.
Selection and peer-review under responsibility of SINTEF Energi AS

Keywords: offshore wind energy; floating wind turbines; control system fault; extreme loads

1. Introduction

As the offshore wind industry moves towards deeper water, floating platforms are an active research and development area worldwide. The majority of the proposed concepts can be categorized as spar-, semi-submersible-, or barge-type hulls, with catenary, taut, or tension leg moorings [1]. Offshore wind turbines will be exposed to a wide range of wind, wave, and electrical conditions during their operational lifetimes, which must be considered in order to establish the structural integrity for both fatigue and ultimate load states [2, 3]. Detailed analyses of operational, fault, and extreme situations are required in order to better understand the performance of different floating platforms and identify critical conditions, especially in the current absence of clear guidelines.

Butterfield et al. provided an early summary of the design challenges related to different types of floating wind turbines [4]. Since then, a wide range of different concepts have been presented, and their advantages

*Corresponding author. Tel.: +47-735-95205
E-mail address: erin.bachynski@ntnu.no.

and disadvantages have been discussed. Previous comparisons of floating wind turbine platforms include several publications from Jonkman and Matha, which considered TLP, spar, and barge concepts [5, 6]. Although these publications include a summary of simulations in normal operation conditions, no quantitative results for fault conditions and extreme load cases were presented due to the “unacceptably large” wind turbine loads [5]. Jonkman and Matha also identified instabilities using the modal analysis computation tool FAST [7] as well as a linear analysis. These instabilities included a platform yaw instability for the barge and TLP when the rotor idled with a blade pitch failure [5, 6]. The current work seeks to provide additional information about the performance of floating wind turbines under fault conditions, using a recently developed non-linear computational tool (Simo-Riflex-AeroDyn) [8].

The occurrence, consequences, detection, and mitigation of wind turbine faults are important research areas, particularly for offshore wind turbines, where maintenance and repair may be complicated by limited access windows [9, Chap. 1]. The blade pitch system was found to be the least reliable sub-assembly in a 1400 turbine-year survey of onshore turbines [9, Chap. 3]. Analyses of both land-based and spar-type wind turbines under pitch system fault conditions have been performed previously. Jiang’s work indicates that certain fault loads may be less significant for spar wind turbines compared to land-based wind turbines, but the effects on the mooring system remain unclear [10]. Different faults may show similar signals, making detection and mitigation more challenging [11].

A sophisticated simulation tool is required to be able to study the transient effect of fault on floating wind turbines. Hansen et al. used HAWC2 and DIgSILENT together to evaluate mechanical loads on a land-based turbine due to grid faults, showing that tower loads may be affected by grid faults and that an open loop simulation is not sufficient to capture the generator speed during such events [12]. A closed loop simulation with DIgSILENT provided some insight into the shaft, tower, and blade loads during grid fault and emergency shutdown of an active stall wind turbine [13]. Although the grid behavior cannot be simulated, the coupled simulation tool Simo-Riflex-AeroDyn is well-suited to account for the hydrodynamic modeling of a range of different platforms, the structural modeling of the wind turbine and mooring systems, the control system for the generator torque and blade pitch, including actuator and measurement errors, and the aerodynamic forces on the blades and tower.

The current work presents the key results from coupled non-linear aero-hydro-servo-elastic simulations of four floating wind turbines: spar, tension leg platform (TLP), a semi-submersible with the turbine on one column, and a semi-submersible with a central tower. Blade seize faults - both uncorrected and also recognized by the controller and followed by shutdown - and grid loss, followed by shutdown, are simulated. In addition to the fault conditions, structural responses in two extreme conditions are considered for comparison. The analysis tools, platform and wind turbine models, environmental conditions, and fault modes are explained in Section 2. Selected responses and a discussion of the key results are provided in Sections 3 and 4, respectively.

2. Methodology

2.1. Coupled Time-Domain Analysis

Three computer codes were used to model the coupled behavior of the floating wind turbine systems in the time domain: Simo modeled the rigid body hydrodynamic forces and moments on the hull [14]; Riflex included the finite element solver, flexible elements for the mooring system, tower, shaft, and blades, and the link to an external controller [15]; and AeroDyn provided the forces and moments on the blades based on Blade Element/Momentum (BEM) or Generalized Dynamic Wake (GDW) theories, including dynamic stall, tower shadow, and skewed inflow correction [16]. The generator torque and blade pitch control system was written in Java. This combination provided a stable non-linear finite element solver, sophisticated hydrodynamics, well-tested aerodynamics, and control logic. The Simo-Riflex wind turbine module has been previously verified [17, 18], and the Simo-Riflex-AeroDyn combination is documented in [8].

Hydrodynamic models and mooring system models depended on the platform. In all of the models, the hull was considered as a rigid body. Added mass, radiation damping, and first order wave forces were obtained from a potential flow model. Additional viscous forces were applied to capture the quadratic damping on the hull and mooring system. Second order forces were present in some models, as noted in sections 2.2.1-2.2.4. Identical

aerodynamic models and structural models of the wind turbine tower and blades were used for all platforms, while the control system was chosen to be appropriate for each platform.

In the aerodynamic load computation, the GDW model with Beddoes-Leishmann dynamic stall was applied to capture the dynamic wake and stall effects, except when the turbine was idling for the entire simulation. For the idling turbine cases, a lookup table of drag and lift coefficients was employed. Drag forces on the tower ($C_D = 1.0$) were applied for all simulations.

The structural model of the tower and blades reflected the properties described in [19, 20]. The 77.6 m tower (from the OC3-Hywind platform description [20]) was modeled with 10 axisymmetric beam elements, while the blades were each modeled with 17 elements with two symmetry axes. The blade model accounted for geometric stiffening, but assumed that the center of gravity, shear center, and elastic center were coincident. Stiffness-proportional damping was applied to approximately match the structural damping specified for the first two independent tower and blade bending modes.

The control system models were based on the NREL-developed controller, as described in [19, 20]. The land-based blade pitch controller constants with constant power above rated wind speed [19] were used for the TLP wind turbine, while the OC3 Hywind control constants with constant torque above rated wind speed [20] were applied for the spar and semi-submersible turbines in order to avoid negative platform pitch feedback in above-rated wind conditions [21].

The coupled dynamic simulation in Simo-Riflex-AeroDyn was carried out in the time domain using Newmark-beta numerical integration ($\beta = 0.256, \gamma = 0.505$) with a time step of 0.005 s. A detailed comparison with HAWC2 for the NREL 5MW wind turbine, both land-based and on the OC3 Hywind spar platform, was performed and indicated good agreement between the two simulation codes.

2.2. Floating Wind Turbine Models

Four floating models are considered here: a spar platform, TLP, and two semi-submersibles, as summarized in Table 1 and depicted in Fig. 1. The platforms are considered in the water depth for which they were designed, ranging from 150 m for the TLP to 320 m for the spar and one semi-submersible. All of the models support the NREL 5MW wind turbine [19] with the OC3 Hywind tower [20] unless otherwise noted in sections 2.2.1-2.2.4.

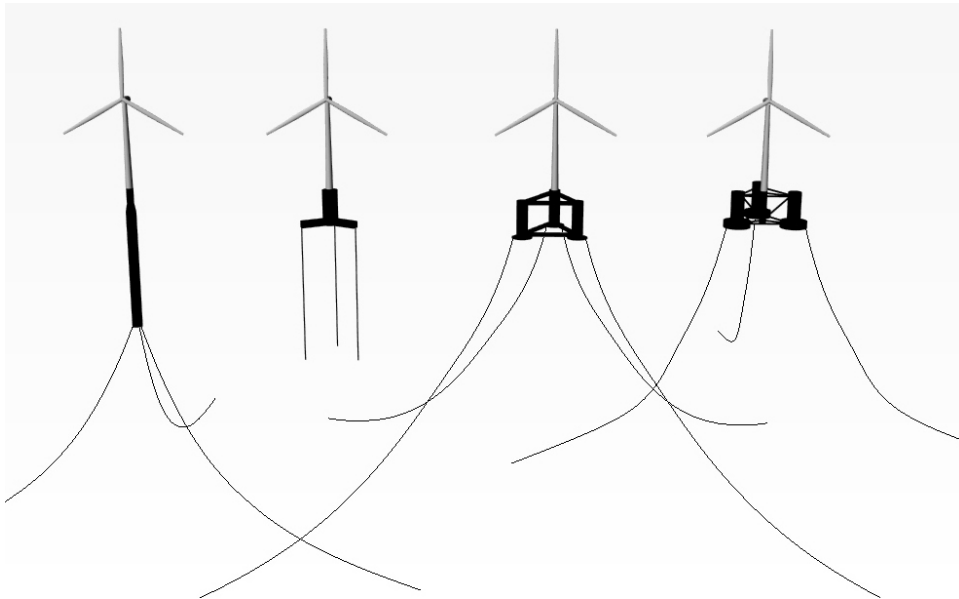


Fig. 1: Floating platform designs: spar, TLP, Semi-Sub 1, and Semi-Sub 2.

Table 1: Floating Platform Models

	Spar	TLP	Semi-Sub 1	Semi-Sub 2
Water depth (m)	320	150	320	200
Displacement (tonnes)	8227	5796	4640	14,260
Hull mass, including ballast (tonnes)	7466	2682	3880	13,473
Draft (m)	120	22	17.0	20.0
Waterline diameter (m)	6.5	14.0	10.0 ^a	12.0/6.5 ^b
Surge natural period (s)	129.5	41.9	99.9	115.9
Sway natural period (s)	129.5	41.9	159.8	115.9
Heave natural period (s)	31.7	0.6	20.0	17.1
Roll natural period (s)	29.7	2.8 ^c	42.1	26.0
Pitch natural period (s)	29.7	2.8 ^c	42.1	26.0
Yaw natural period (s)	8.2	18.0	66.7	80.2

^a Single column

^b Single offset column/Center column

^c Includes tower bending

2.2.1. Spar Platform

The spar platform considered here was the OC3 Hywind hull, as defined by Jonkman, with 120 m draft in 320 m water depth [20]. In addition to the first order and viscous forces, mean wave drift forces were applied and Newman's approximation was used to estimate the difference-frequency wave excitation.

A chain mooring system with delta lines and clump weights was applied to approximate the mooring system stiffness described in [20], which specifies only the resulting stiffnesses, not the components. The mooring lines were modeled using bar elements and connecting joints, allowing for a full dynamic solution.

2.2.2. Tension Leg Platform

The TLP model considered here was an approximately half-scale version of the original Sea Star oil platform [22]. Approximately 60% of the displacement came from the center column, with the rest coming from the pontoons. Additional details regarding this design can be found in [23], where it is identified as TLPWT 3. The platform displacement is approximately one-half that of the MIT-NREL TLP [24], and approximately twice that of the UMaine TLP [25].

In addition to the first order and viscous forces, difference-frequency forces using Newman's approximation and sum-frequency forces due to the second order potential model were also applied.

The tendons were modeled using axisymmetric beam elements. Hydrodynamic forces on the tendons were applied using Morison's equation. The tendons are somewhat stiffer than those described in, for example, [24, 25], giving the platform very short natural periods in heave and pitch.

2.2.3. Semi-Submersible Platform 1

This study includes a semi-submersible with the turbine placed on one of the three columns. The platform specifications and mooring system are similar, but not identical, to the WindFloat platform. The geometry and the original mass model are identical, and the mooring system gives similar natural periods to the generic WindFloat specification [26].

WindFloat has an active ballast system that counteracts the rotor's thrust force and makes the platform float upright. The reaction time of this system is 20 minutes according to Roddier [26]. The aerodynamic loads on the rotor differ significantly from the upright position when the rotor is tilted, so the ballast system was included in the numerical model. This was done by making the mass model a function of the mean wind speed, i.e. by giving different mass and restoring matrices for each environmental condition. Assuming that the dynamic effects of slowly changing ballast are small, mass and restoring were kept constant through each time domain simulation. The ballast model also counteracts the rotor torque moment.

2.2.4. Semi-Submersible Platform 2

The second semi-submersible concept is the OC4 DeepCWind semi-submersible, as described in detail in [27]. The wind turbine is located on a center column. There are three offset columns with pontoons around the center column, each of which has an attached catenary mooring line. Braces are used to connect all of the columns as an integrated body. The large waterplane area moment of inertia provides good stability and stiffness, thus limiting the platform pitch angle in wind and waves. The OC4 DeepCWind semi-submersible's large displacement was chosen to give it a long natural period in heave.

2.3. Environmental and Fault Conditions

Seven wind and wave conditions were simulated, as summarized in Table 2. All of the environmental conditions (ECs) considered correlated, directionally aligned wind and waves for the North Sea, where the correlation of wind and waves follows [28]. ECs 1-5 represented a range of typical operational conditions. EC 6 was a storm condition, where the turbine idled, and EC 7 was an extreme turbulence condition close to the maximum thrust condition.

The number and length of simulations were chosen in order to provide a reasonable statistical basis for comparison. In extreme cases, where the load maxima were expected to be driven by waves or lower-frequency wind variations, six three hour simulations were considered. For fault cases, where the deterministic fault event is expected to dominate, 30 shorter simulations were carried out. Current offshore wind turbine standards suggest that 12 10-minute simulations be carried out for power production plus fault cases [3], but 30 simulations were employed here in order to capture some of the significant stochastic and azimuthal variation that have been noticed in previous work [10].

Three-dimensional turbulent wind fields were generated in NREL's TurbSim program [29] based on the Kaimal spectrum for IEC Class C [2]. The normal turbulence model (NTM) was used for ECs 1-6, while the extreme turbulence model (ETM) for class III turbines was used for EC 7. The wind shear was modeled by the power law with exponent 0.14 [3]. In the vertical plane 32x32 points were used over an area of 160m x 160m, with wind field generation time step 0.05 seconds.

The simulated wave series were generated based on JONSWAP spectra, where the peak enhancement factor depends on the significant wave height (H_s) and peak period (T_p) [14]. A frequency discretization of 0.002 rad/s was used.

Table 2: Combined wind and wave simulation conditions

	U_w (m/s)	H_s (m)	T_p (s)	Turb. Model	Fault Considered	Num. of Seeds	Sim. Length (s)
EC 1	8.0	2.5	9.8	NTM	A, B, C, D	30	1000
EC 2	11.2	3.1	10.1	NTM	A, B, C, D	30	1000
EC 3	14.0	3.6	10.3	NTM	A, B, C, D	30	1000
EC 4	17.0	4.2	10.5	NTM	A, B, C, D	30	1000
EC 5	20.0	4.8	10.8	NTM	A, B, C, D	30	1000
EC 6	49.0	14.1	13.3	NTM	A (idling)	6	10800
EC 7	11.2	3.1	10.1	ETM	A	6	10800

The fault conditions are defined as:

1. A) Fault-free condition: normal power generation in ECs 1-5 and 7, idling in EC 6.
2. B) Blade seize: the pitch actuator of one blade is blocked at time $TF = 400$ s and the turbine continues to operate, with the controller trying to maintain the rotation speed by pitching the other two blades.
3. C) Blade seize followed by shutdown: the pitch actuator of one blade is blocked at time $TF = 400$ s, and the controller reacts by shutting down $TD = 0.1$ s later.
4. D) Grid loss followed by shutdown: the grid is disconnected at time $TF = 400$ s, and the controller reacts by shutting down $TD = 0.1$ s later.

When shutdown occurs, the grid is disconnected and all blades with working actuators are pitched to feather (90°) at the pitch rate PR . In the current work, the pitch rate during shutdown is chosen to be $PR = 8$ deg/s, the maximum pitch rate suggested in [19]. The pitch rate can have a significant impact on the loads and motions: for a spar platform, a faster pitch rate tends to decrease the motions but increase the rotor loads [10].

For fault cases B, C, and D, the fault occurred after 400 seconds of normal operation. An additional 600 seconds after fault were simulated in order to capture several subsequent cycles of low-frequency events. For cases C and D, $TD = 0.1$ seconds, which is approximately 10 times the sampling frequency of the controller [30].

An example of the wind turbine behavior during fault case C is illustrated in Fig. 2. As shown, the non-faulted blades reached full feather within approximately 10 seconds, and the turbine slowed down within 20 seconds. During shutdown without blade pitch fault, the turbine stopped within 12 seconds. Fig. 2 also shows the characteristic negative thrust and torque during shutdown. The fast pitching action pulled the rotor back into the wind, and these peaks were even more pronounced during shutdown without blade pitch fault.

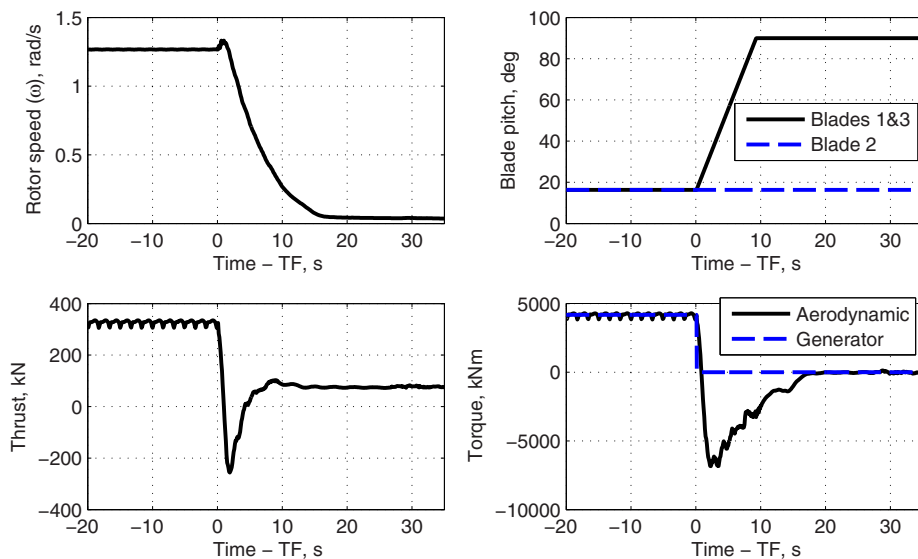


Fig. 2: Fixed wind turbine: blade 2 seize followed by shutdown (case C). Constant wind, 20 m/s.

3. Results

3.1. Response Maxima

Choosing a consistent method to define maxima is particularly challenging when comparing the fault-induced response, which is a short-term response and often dominated by the transients in the shut-down procedure, and the response in an extreme sea state, which is considered to last for three hours at a time. Adding to the complication is the azimuth dependence of some fault-induced responses (particularly fault case C). Two different methods were considered:

1. Absolute maximum: largest absolute value encountered in all 30 1000-second simulations (ECs 1-5), or all 6 3-hour simulations (ECs 6-7)
2. Expected maximum: average of the largest absolute value encountered in each of the 30 1000-second simulations (ECs 1-5) or 6 3-hour simulations (ECs 6-7).

Table 3 shows the environmental condition and fault condition leading to the largest responses using both definitions. The responses considered include the global motions, the moments at the tower top and base in the

fore-aft (FA) and side-side (SS) directions, blade root bending moments in the local coordinate system, and the mooring system loads. The most severe mooring system loads were evaluated in different ways for different concepts. For the spar, the tension in the delta lines was measured, while the minimum tendon tension was considered for the TLP. The fairlead tension was considered for the semi-submersibles.

Table 3: Load cases resulting in the absolute maxima (1)/ largest expected maxima (2). Note: blade 2 is the faulted blade for type B and C faults.

Response	Land-based	Spar	TLP	Semi-Sub 1	Semi-Sub 2
Surge	-	6A/6A	6A/6A	6A/7A	6A/6A
Sway	-	6A/6A	6A/6A	5C/5C	5C/5C
Heave	-	6A/6A	6A/6A	6A/6A	6A/6A
Roll	-	6A/6A	6A/6A	5C/5C	5C/6A
Pitch	-	6A/6A	6A/6A	2D/2D	6A/6A
Yaw	-	6A/6A	5C/5C	5C/5C	7A/7A
Tower Base Fore-Aft Moment	2C/2D	6A/6A	6A/6A	6A/2D	6A/6A
Tower Base Side-Side Moment	5C/5C	6A/6A	5C/4C	5C/5C	6A/6A
Tower Top Fore-Aft Moment	2C/2C	2C/2C	3C/2C	2C/2C	2C/2C
Tower Top Side-Side Moment	5B/5B	4B/5B	5B/5B	5B/5B	5B/6A
Blade 1 Flapwise Moment	4B/7A	4B/7A	5B/7A	3B/7A	4B/7A
Blade 1 Edgewise Moment	2C/2D	2C/2C	3C/3D	4D/3C	6A/6A
Blade 3 Flapwise Moment	4B/7A	4B/7A	5B/7A	3B/7A	3B/7A
Blade 3 Edgewise Moment	2D/2D	3D/5D	2D/4D	3D/5D	6A/6A
Blade 2 Flapwise Moment	3B/7A	3B/7A	5B/7A	2B/7A	3B/2B
Blade 2 Edgewise Moment	3D/3D	5D/3D	2D/3D	4D/2D	6A/6A
Mooring system	-	6A/6A	6A/6A	6A/6A	6A/6A

Table 3 highlights several important results.

1. The global motions and (consequently) the mooring loads were dominated by the extreme wave condition (6A), while blade and tower top bending moments were more affected by fault conditions.
2. The absolute extreme blade bending loads tended to occur in fault conditions. Flapwise loads were particularly sensitive to imbalance (B), while edgewise loads were most sensitive to shutdown (fault types C and D).
3. The extreme blade bending moments depended on the extreme value computation method. While fault conditions might yield the absolute extreme value, the expected maximum value for flapwise loads tended to occur in the extreme turbulence condition (7A). It is important to note that the expected maxima for conditions 6 and 7 effectively represent 3.6 times longer time series than the fault conditions. Furthermore, the maximum blade edgewise bending moments can depend on the azimuth angle at the time of shutdown (see also [10]). Averaging over the randomly distributed azimuth angles for different fault conditions does not necessarily give a good estimate of the condition which will lead to the absolute extreme value.
4. The tower top bending moments, which are representative of the shaft loading, were sensitive to imbalance loads. The fore-aft tower top loads were dominated by blade imbalance followed by shutdown in near-rated conditions, while side-side tower top loads were dominated by blade imbalance at higher wind speeds.

It is important to note, however, that Table 3 does not give any indication of the relative severity of different loads, nor does it show the statistical variation present in the extreme values. An illustration of the statistical variation in the maximum value for different simulations is shown in Fig. 3. For each environmental and fault condition, the range of the single-simulation maximum absolute value of the fore-aft tower bending moments is shown. The responses in Fig. 3 are normalized by the expected absolute value for each condition.

There was significant stochastic variation in the maxima computed for individual simulations – particularly for fault types B and C, where rotor imbalance was present. In some cases, the absolute maximum was up to 50%

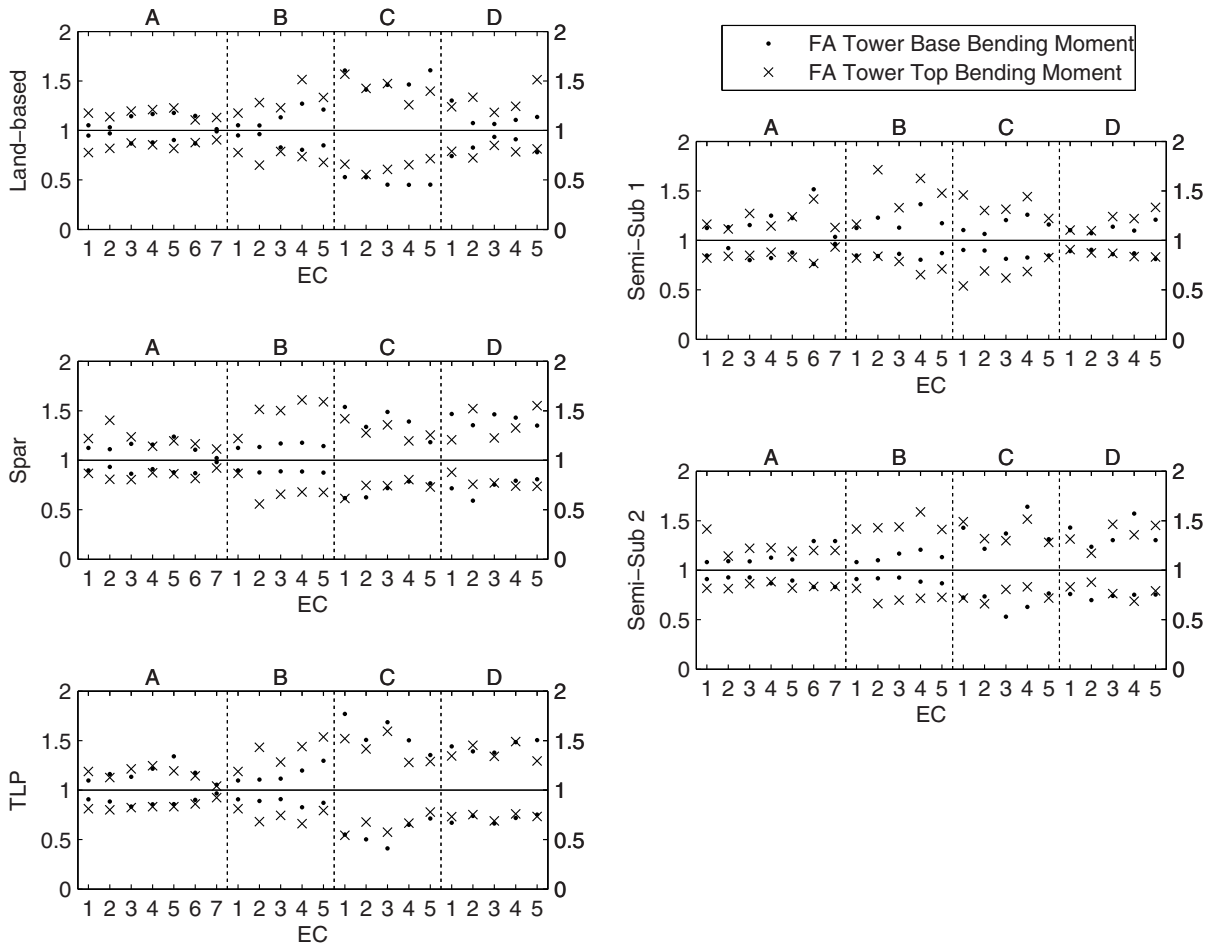


Fig. 3: Range of absolute maximum response values for different seeds. Response values are divided by the expected value of the maximum for each fault type (A-D) and EC (1-7).

larger than the average of the maxima. The relative variation in the maxima tended to be larger at the tower top than at the base for cases A and B, but large variations were seen at both locations.

Despite the large variation in maxima, there were some clear patterns in the responses. The following subsections (3.2-3.5) discuss the interesting consequences of pitch actuator fault, grid loss, and shutdown on the motions, mooring system loads, tower loads, and blade loads of floating wind turbines.

3.2. Platform Motions and Mooring System Loads

With a few exceptions, the platform motions - and the related mooring system loads - were not very sensitive to fault. The heave motions were wave-driven and unaffected by fault.

The decreased thrust resulted in decreased surge motion for all platforms, and in decreased pitch motion for all platforms except for semi-sub 1 during shutdown. Due to semi-sub 1's low restoring stiffness in pitch, the

sudden decrease in thrust attributed to shutdown resulted in a large static pitch angle of up to 12.5 deg, preceded by a larger dynamic pitch. The ballast system, which would correct for this change, is assumed to require at least 20 minutes to take effect [26]. Fig. 4 compares the pitch motions during one simulation of case 3C for the spar and semi-submersible designs. As shown, the spar and semi-sub 2 operate with small mean pitch in normal conditions and return to near zero pitch after shutdown. Semi-sub 1 operates with near zero mean pitch during normal conditions and experiences large pitch motion after shutdown. It should be noted that the semi-sub 1 model is not an exact representation of the WindFloat concept: increased restoring stiffness, increased damping, and different control actions may serve to mitigate the large response.

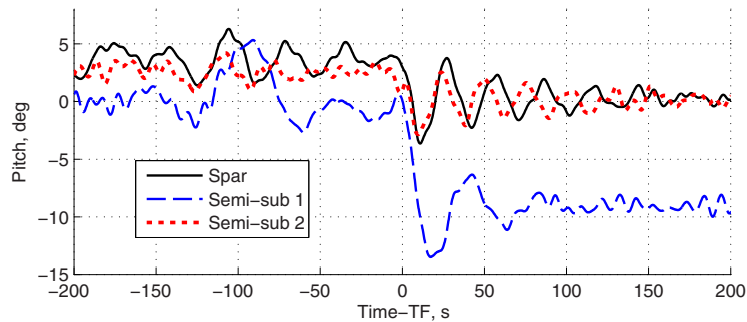


Fig. 4: Spar, semi-sub 1, and semi-sub 2 pitch motion, case 3D.

The sway, roll, and yaw motions are all related. During normal operation, variations in the rotor torque can induce roll motion, which can then induce yaw through both wave forces and thrust forces. Additionally, uneven wind across the rotor can induce yaw moments. Although sway, roll, and yaw motions are typically small, imbalance loads can be important. During blade seize, the yaw motions increased slightly for the TLP (5-10%) and even more for the spar (up to 50%). Blade seize followed by shutdown (case C) caused even larger yaw motions for the spar and TLP. The semi-submersible concepts have large moments of inertia in yaw, but the spar and TLP have small inertia and relatively high stiffness, making them responsive to the aerodynamic impulse load. Compared to their normal operation, yaw motions increased by approximately 25% for the TLP (maximum expected fault-induced yaw of up to 2.9 degrees) and almost 400% for the spar (7.3 degrees). The spar experienced only slightly larger yaw motion in the extreme condition (expected maximum 8.3 degrees).

Since the semi-submersible mooring lines were most sensible to surge motion and the TLP tendons were most sensitive to platform pitch motion, the mooring loads generally decreased following fault. Both yaw and surge motion could be important for the spar. The yaw motions due to blade seize caused a 12.5% increase in delta line tension for the spar, while blade seize followed by shutdown led to a 50% increase compared to operational loads. The largest fault-induced mooring loads occurred near the rated condition. The storm-induced loads were, however, still larger (60% larger than operational loads).

3.3. Tower Base Bending Moments

The fore-aft tower base bending moment is driven by the thrust force and by the weight of the rotor, which can cause a large bending moment due to platform pitch or tower bending. For the spar, TLP, and semi-sub 2 platforms, shutdown resulted in decreased fore-aft loading due to the decreased thrust, while blade seize had little effect. Shutdown, however, caused relatively large fore-aft tower base bending loads for both the land-based and semi-sub 1 platforms. For the land-based platform, the sudden change in the thrust caused relatively large loading at the tower base and lightly-damped vibrations in the first bending mode. The semi-sub 1 platform experienced large tower base loads due to the large pitch angle described in Sec. 3.2.

The side-side tower base bending moment depended on the torque moment at the top of the tower and the rotor weight (due to roll motions or side-side bending). During normal operation, this moment is much smaller than the fore-aft moment. For all of the platforms, a small increase (5-10%) in the loading was observed during blade seize (case B), while shutdown mitigated the loads.

3.4. Tower Top Bending Moments

The tower top bending moments, which reflect both aerodynamic loads and loads due to rotor inertia, may be seen as a measure of the drivetrain loads, particularly the shaft bending moments. These loads are known to be larger for floating systems compared to land-based or fixed bottom turbines [31]. The current study indicated that grid loss and shutdown would not lead to especially large loads, but blade seize - with or without shutdown - could lead to critical load conditions for some platforms.

Figs. 5 and 6 compare the expected maximum fore-aft and side-side bending moments, respectively, for all of the concepts and all of the environmental conditions. As shown, blade seize increased both the fore-aft and side-side bending moments, particularly in higher wind speeds.

Shutting down the turbine after blade seize error (C) tended to reduce the expected maximum fore-aft moment in high wind speeds for the land-based and TLP wind turbines, but tended to increase the maximum load in lower wind speeds. Shutting down the turbine in high wind speeds was less effective for the spar and semi-sub platforms.

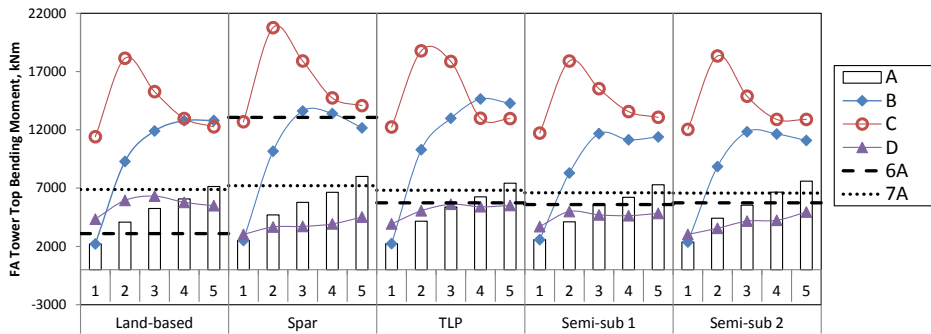


Fig. 5: Expected maximum tower top fore-aft (FA) bending moment for all platforms and conditions. ECs 1-5 are shown with bars (A), diamonds (B), open circles (C), and triangles (D). The expected maxima for ECs 6 and 7 for each concept are shown as horizontal lines for comparison.

As shown in Fig. 6, the side-side bending moment at the tower top was fairly consistent across all platforms. Shutting down the platform gave a clear load reduction of the side-side bending moment for all platforms compared to the continued operation with a seized blade.

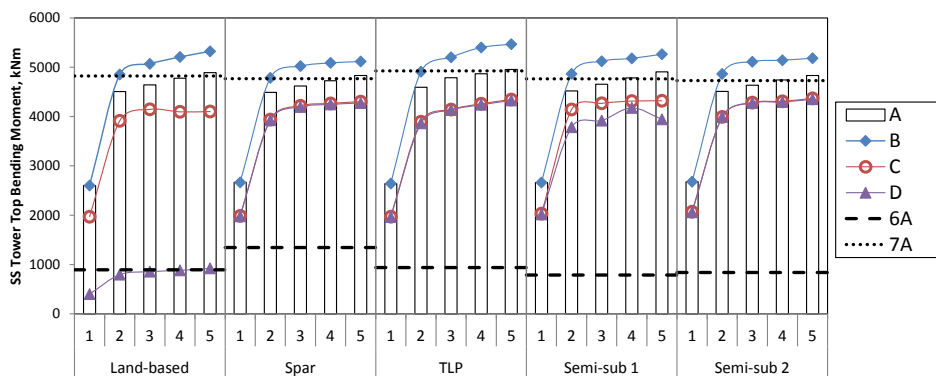


Fig. 6: Expected maximum tower top side-side (SS) bending moment for all platforms and conditions. ECs 1-5 are shown with bars (A), diamonds (B), open circles (C), and triangles (D). The expected maxima for ECs 6 and 7 for each concept are shown as horizontal lines for comparison.

The nature of the maximum fore-aft load in fault cases B and C is illustrated in Fig. 7. When shutdown occurred, the maximum load was encountered within a short period immediately after shutdown began, followed

by a reduction in the load. The maximum load in case B, on the other hand, took more time to develop. If the blade pitch error were to persist even longer, larger loads than those seen here might be expected, especially for the spar and semi-submersible designs, which have longer pitch periods than the TLP.

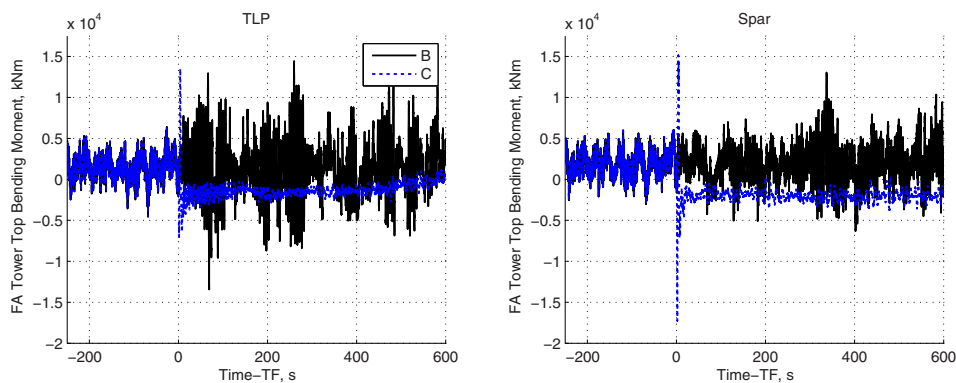


Fig. 7: Spar and TLP fore-aft (FA) tower top bending moment for one realization of EC 5 (cases B and C).

3.5. Blade Root Bending Moments.

The flapwise and edgewise bending moments at the blade root were considered in this study. During normal operation, the flapwise bending moment - the larger of the two moments - is dominated by aerodynamic loads, while gravity loading is the primary contributor to the edgewise loads. In general, the effects of faults and shutdown on the blade loads were similar for all of the platforms.

The flapwise bending moment was susceptible to blade seize faults, while shutdown decreased the loading. Compared to normal operation conditions, blade seize faults (case B) caused small (5-10%) increases in the expected maximum flapwise loads on the faulted blade and somewhat larger (up to 25%) increases for the other two blades. Since the controller continues to try to maintain the rotation speed, the chosen pitch angles for the non-faulted blades may result in larger loads. It is expected that longer simulations with fault case B would result in even larger load increases.

The edgewise bending moment was not affected by blade seize faults, but was sensitive to shutdown. The shutdown process yielded maximum loads up to 40% more than the normal operational condition. This increase was observed for all platforms and tended to be maximum near the rated wind speed.

4. Discussion

The present study employed a coupled non-linear time domain computer simulation program to investigate the effects of blade pitch faults and shutdown on several floating wind turbines. Although extreme weather conditions were found to generally result in more severe motions, mooring loads, and tower base loads, fault conditions were critical in some cases for tower top and blade loads. Furthermore, fault and shutdown may have important effects on certain platforms in given conditions: large yaw motions for the studied spar and TLP, and large pitch as a consequence of shutdown for the semi-sub 1 platform.

No unstable behavior was encountered in the simulation of the floating platforms under fault conditions. The nonlinear simulation tool did not reproduce the instability identified by [5, 6] for the TLP idling with a blade pitch fault in fault case C after shutdown.

These results must be considered in the light of certain assumptions and limitations. Only aligned wind and wave conditions were considered, although misaligned wind and waves may be a severe loading condition for floating wind turbines [6, 32]. Misalignment, and misalignment exacerbated by fault, should be considered in future studies.

The hydrodynamic models of the semi-submersibles did not include mean wave drift forces, which are expected to increase the maximum surge motions - and corresponding mooring system loads - in large waves. Damping in the numerical method should also be carefully investigated, and comparisons to real-world data should be carried out when possible to better investigate the blade and tower vibrations.

A limited number of realizations of each fault were carried out. There are large stochastic variations - and uncertainties - related to the maximum loads induced by fault events. Some of the variation is related to azimuthal variations, while additional uncertainties are related to the stochastic wind and waves (and the phase angle between the platform response and the incoming wind and waves).

The influence of the controller reaction time was not studied in the present work. The controller reaction time will also influence the azimuth angle at the time of shutdown, and can therefore have a significant effect on the loads for fault cases C and D. Furthermore, a slower reaction time will result in additional overspeed during grid faults, which is an important consideration for both fixed and floating wind turbines.

Further study of fault-induced loads on floating wind turbines should explain the load mechanisms in greater detail by examining the mechanism by which blade pitch error affects the other blades, considering the azimuthal variation during shutdown, and carrying out the case B simulations for a longer period after fault. More refined structural models could address the effect of the large increases in tower top loads on the drivetrain components. Additionally, different control strategies - such as varying the pitch rate during shutdown or waiting for a particular azimuthal position before starting shutdown - could be investigated as methods to reduce the tower top and blade loads.

5. Acknowledgments

The authors gratefully acknowledge the financial support from the Research Council of Norway granted through the Centre for Ships and Ocean Structures, and Norwegian Research Centre for Offshore Wind Technology (NOWITECH), NTNU. Erin E. Bachynski acknowledges support from Statoil through an MIT-NTNU Gemini cooperative research project. Thanks are extended to Zhiyu Jiang for his discussions and comments.

References

- [1] Moan T, Gao Z, Karimirad M, Bachynski EE, Etemaddar M, Jiang Z, et al. Recent Developments of the Design and Analysis of Floating Wind Turbines. In: ISCOT: Developments In Fixed & Floating Offshore Structures. Busan, Korea: The Royal Institution of Naval Architects; 2012.
- [2] International Electrotechnical Commission. Wind turbines: Part 1: Design Requirements; 2005. IEC61400-1:2005(E).
- [3] International Electrotechnical Commission. Wind turbines: Part 3: Design requirements for offshore wind turbines; 2009. IEC61400-3.
- [4] Butterfield S, Musial W, Jonkman J, Sclavounous P, Wayman L. Engineering Challenges for Floating Offshore Wind Turbines. In: 2005 Copenhagen Offshore Wind Conference. NREL/CP-500-38776. Copenhagen, Denmark; 2005.
- [5] Jonkman J, Matha D. A Quantitative Comparison of the Responses of Three Floating Platforms. In: European Offshore Wind 2009 Conference and Exhibition. Stockholm, Sweden; 2009.
- [6] Jonkman JM, Matha D. Dynamics of offshore floating wind turbines. *Wind Energy*. 2011;14:557–569.
- [7] Jonkman JM, Buhl ML Jr. FAST User's Guide. National Renewable Energy Laboratory; 2005. NREL/EL-500-38230.
- [8] Ormberg H, Bachynski EE. Global analysis of floating wind turbines: Code development, model sensitivity and benchmark study. In: The 22nd International Ocean and Polar Engineering Conference. Rhodes, Greece: International Society of Offshore and Polar Engineers; 2012.
- [9] Tavner P. Offshore Wind Turbines: Reliability, availability and maintenance. No. 13 in Renewable Energy Series. The Institution of Engineering and Technology; 2012.
- [10] Jiang Z, Karimirad M, Moan T. Dynamic response analysis of wind turbines under blade pitch system fault, grid loss and shut down events. *Wind Energy*. 2013; Accepted for publication.
- [11] Etemaddar M, Gao Z, Moan T. Structural Load Analysis of a Wind Turbine under Pitch Actuator and Controller Faults. In: The Science of Making Torque from Wind. Oldenburg, Germany; 2012.
- [12] Hansen AD, Cutululis NA, Sørensen P, Iov F, Larsen TJ. Simulation of a flexible wind turbine response to a grid fault. In: European Wind Energy Conference & Exhibition. Berlin, Germany; 2007.
- [13] Cutululis NA, Hansen AD, Iov F, Sørensen P. Grid Faults Impact on the Mechanical Loads of Active Stall Wind Turbine. In: Second International Symposium on Electrical and Electronics Engineering (ISEEE-2008). Galati, Romania; 2008.
- [14] MARINTEK. SIMO User's Manual; 2011.
- [15] MARINTEK. RIFLEX User's Manual; 2011.

- [16] Moriarty PJ, Hansen AC. AeroDyn Theory Manual; 2005. NREL/TP-500-36881.
- [17] Luxcey N, Ormberg H, Passano E. Global Analysis of a Floating Wind Turbine Using an Aero-Hydro-Elastic Numerical Model. Part 2: Benchmark Study. In: 30th International Conference on Ocean, Offshore, and Arctic Engineering. OMAE2011-50088. Rotterdam, the Netherlands; 2011.
- [18] Ormberg H, Passano E, Luxcey N. Global Analysis of a Floating Wind Turbine Using an Aero-Hydro-Elastic Model: Part 1: Code Development and Case Study. In: 30th International Conference on Ocean, Offshore, and Arctic Engineering. OMAE2011-50114. Rotterdam, the Netherlands; 2011.
- [19] Jonkman J, Butterfield S, Musial W, Scott G. Definition of a 5-MW Reference Wind Turbine for Offshore System Development. National Renewable Energy Laboratory; 2009. NREL/TP-500-38060.
- [20] Jonkman J. Definition of the Floating System for Phase IV of OC3; 2010. NREL/TLP-500-47535.
- [21] Larsen TJ, Hanson TD. A method to avoid negative damped low frequent tower vibrations for a floating, pitch controlled wind turbine. Journal of Physics: Conference Series, The Second Conference on The Science of Making Torque from Wind. 2007;75.
- [22] Kibbee SE, Leverette SJ, Davies KB, Matten RB. Morpeth SeaStar Mini-TLP. In: Offshore Technology Conference. OTC 10855; 1999.
- [23] Bachynski EE, Moan T. Design Considerations for Tension Leg Platform Wind Turbines. Marine Structures. 2012;29:89–114.
- [24] Matha D. Model Development and Loads Analysis of an Offshore Wind Turbine on a Tension Leg Platform, with a Comparison to Other Floating Turbine Concepts. University of Colorado-Boulder; 2009.
- [25] Stewart G, Lackner M, Robertson A, Jonkman J, Goupee A. Calibration and Validation of a FAST Floating Wind Turbine Model of the DeepCwind Scaled Tension-Leg Platform. In: 22nd International Offshore and Polar Engineering Conference. NREL/CP-5000-54822. Rhodes, Greece: International Society of Offshore and Polar Engineers; 2012.
- [26] Roddier D, Peiffer A, Aubault A, Weinstein J. A Generic 5MW WindFloat for Numerical Tool Validation and Comparison Against a Generic Spar. In: 30th International Conference on Ocean, Offshore and Arctic Engineering. OMAE2011-50278. Rotterdam, the Netherlands; 2011.
- [27] Robertson A, Jonkman J, Masciola M, Song H, Goupee A, Coulling A, et al. Definition of the Semisubmersible Floating System for Phase II of OC4; 2012.
- [28] Johannessen K, Meling TS, Haver S. Joint Distribution for wind and waves in the Northern North Sea. In: The 11th International Offshore and Polar Engineering Conference & Exhibition. Stavanger, Norway: International Society of Offshore and Polar Engineers; 2001.
- [29] Jonkman BJ. TurbSim User's Guide: Version 1.50. National Renewable Energy Laboratory; 2009. NREL/TP-500-46198.
- [30] Odgaard PF, Stoustrup J, Kinnaert M. Fault Tolerant Control of Wind Turbines a benchmark model. In: 7th IFAC Symposium on Fault Detection, Supervision and Safety of Technical Processes. Barcelona, Spain; 2009. p. 155–160.
- [31] Xing Y, Karimirad M, Moan T. Modelling and analysis of floating spar-type wind turbine drivetrain. Wind Energy. 2013; Accepted for publication.
- [32] Jiang Z, Karimirad M, Moan T. Steady State Response of a Parked Spar-type Wind Turbine Considering Blade Pitch Mechanism Fault. In: The 22nd International Ocean and Polar Engineering Conference. Rhodes, Greece: International Society of Offshore and Polar Engineers; 2012.